Electronic supplementary materials *Mendeleev Commun.*, 2021, **31**, 227–229

Irradiation of detonation nanodiamonds with γ-rays does not produce long living spin radicals

Vladimir Yu. Osipov, **Nikolai M. Romanov and Kazuyuki Takai**

Contents

S1. General information and Experimental Procedures

Purification. Commercial DND powder was purified in boiling 35% hydrochloric acid step by step (4-5 times) and thereafter washed in boiling distilled deionized water (4-5 times) for removal iron, iron-related complexes and other *3d*- ferromagnetic impurities. The dense sedimented part of DND suspension (pellet) was thereafter dried in secondary vacuum at 110 ºC. The details of such procedure were described earlier in Ref.S1.

Sorption. The surface of acid-treated DND particles in aggregates is terminated by oxygen-containing groups [S2]. The average pore size is 4.5 nm in such DND aggregates [S3]. The specific surface area of DND is about ~240 m^2/g. Such a surface is lyophilic and readily absorbs water on the surface and in the interparticle voids between adjacent particles [S3-S5]. Dry DND powder adsorbs a noticeable amount of volatile components - water, oxygen, nitrogen and hydrocarbons from the atmosphere. Oxygen and nitrogen are physisorbed mainly on sp^2 fragments on the surface, and water on hydrophilic adsorption sites of the DND surface (oxygen-containing carboxyl and hydroxyl groups). In this case, the role of nitrogen is to block physisorption sites for oxygen binding. We emphasize that the main sorbed agent is water molecules, and to a lesser extent molecular oxygen and nitrogen [S4,S5]. The presence of molecular oxygen in the triplet state with spin 1 is proved by a small change (up to 4%) in the peak intensity of the DND EPR signal during vacuum pumping. The weight of the adsorbates, measured from the difference in the weights of the powders after prolonged storage in air and annealing in vacuum at 470 °C for 5-7 hours, was about ~7-8% of the weight of the DND powder. This is evidence of the presence of physisorbed molecular clusters on the DND surface [S6], the weight of which is also the main source of inaccuracy in determining the weight concentration of paramagnetic centers in DND.

Sample pre-treatment. The acid-treated DND powder (weight ~59 mg) of grey colour was packed in a thin aluminium foil (30 mg capsule) and placed in the middle of a Pyrex glass tube with an outer diameter of 5 mm and a length of ~22 cm (see Figure S1). The sample in Pyrex tube was preliminary heat treated at temperature ~400 ºC and pressure ~2.1×10^{-6} Torr during 5-6 hrs for removal adsorbed water, dioxygen and other physisorbed molecules. Careful removal of air inside the Pyrex tube and even the adsorbed oxygen from DND surface is a key requirement for precise magnetic measurements at low temperatures because O_2 molecules are paramagnetic and disturb magnetic data through their parasitic condensation below ~55 K. The open end of tube was sealed

at pressure ~2.1×10^{-6} Torr after the end of heat treatment. Magnetic susceptibility measurements were done with SQUID magnetometer MPMS-7 (Quantum Design, US). Temperature dependence

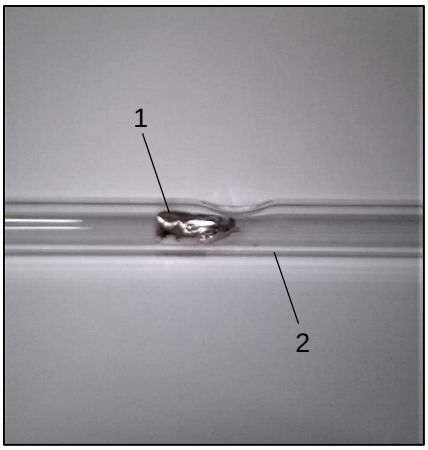

Figure S1 Image of DND powder packed in a thin metal foil (1) and placed in the middle of a long Pyrex glass tube (2) with an outer diameter of 5 mm. The left and right parts of tube are not shown in the figure. The contrast of the image has been specially increased for better viewing.

of magnetic susceptibility was measured in magnetic field 0.9 T in the range 2-300 K while the magnetization curve was measured at lowest achievable temperature T=2 K.

S2. Magnetic susceptibility data, Formulas and Spin concentration

Magnetisation of acid-purified metal-free nanodiamond in an arbitrary magnetic field is a sum of two components:

$$M(H) = \chi_o H + M_{\mathrm{DND}}^{S_1=1/2} = \chi_o H + N_{s_1} g S_1 \mu_B B_{S=\frac{1}{2}}(H)$$

whereas the magnetic susceptibility measured in low (< 1 T) magnetic fields is:

$$\chi = \frac{M}{H} = \chi_0 + \frac{C}{T-\Theta}$$

here χ_o – temperature independent core diamagnetic susceptibility of carbon atoms, here χ_0 can be accurately determined from the temperature behavior χ–T of the total magnetic susceptibility: $\chi(T) = \chi_0 + \chi_{\mathrm{CW}}(T)$, where the temperature-dependent term χ_{CW} for the group of only interior spins follows the Curie-Weiss law (see below), H- applied magnetic field, N_{s_1}- concentration of interior S_1=1/2 paramagnetic species inside the DND particles, S_1 – spin value for paramagnetic species related with own interior defects of DND particles, μ_B – Bohr magneton, $B_{S=\frac{1}{2}}(H)$ – Brillouin function for the ensemble of spins with spin values ½ , C- Curie constant, T – sample temperature and Θ is a Weiss temperature. $g \approx 2$ is a g-factor (Lande factor) for main spin-half paramagnetic species. Brillouin function for spin S species is defined by the next expression [S7]: $B_S = \frac{2S+1}{2S}\coth\frac{(2S+1)x}{2} - \frac{1}{2S}\coth\frac{x}{2}$, where S is a spin value and variable x equals $x = g\mu_B H/k_B T$. Here k_B is a Boltzmann constant. At T = 2 K Brillouin function shows the saturation trend. The saturation trend is more featured for higher spin values. Brillouin function fits well the experimental magnetization curve related with only localized spins if we assume the next fitting parameters: S=1/2, T =2.07 K and N_{s_1} = 5.90×10^{19} spins ·g^{-1}. S=1/2 value means that the main

paramagnetic species of DND are dangling bond spins related with broken interior C-C, C-N and other exterior C-C, C-O, C-H bonds.

The χ_o – value required for the above estimate was obtained from an analysis of the temperature behavior of the DND magnetic susceptibility $\chi = M/H$ at H = 0.9 T in the range 2-300 K. By plotting the reciprocal susceptibility $(\chi - \chi_0)^{-1}$ vs the temperature it was possible to find χ_o as a fitting parameter when such plot looks as an ideally straight line (Figure S2). We found χ_o =- 0.418×10^{-6} emu/(Oe·g).

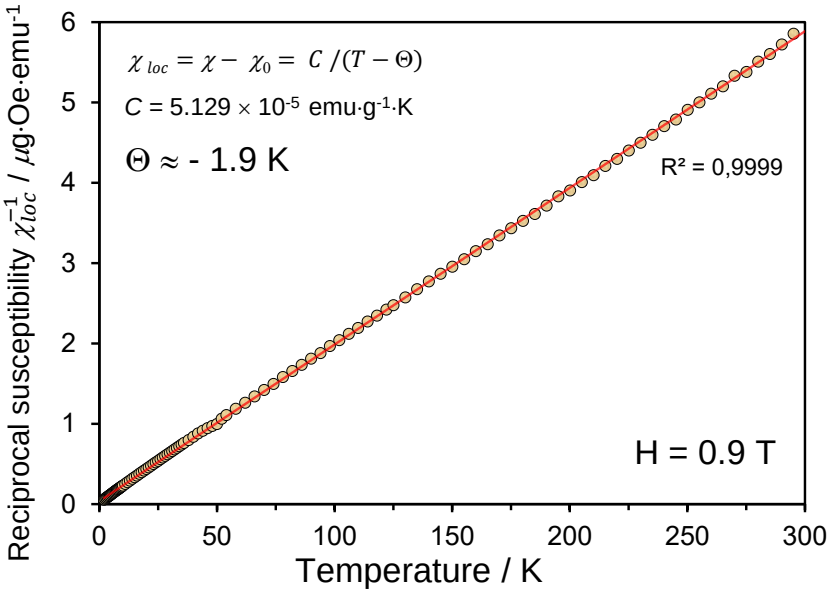

Figure S2 Temperature dependence of reciprocal magnetic susceptibility of only localized spins measured in magnetic field 0.9 T. The contribution from container (aluminium foil) was specially subtracted from the total magnetization. Yellow circles – experimental points, red line – theoretical fitting by straight line with C = 5.129×10^{-5} emu·g^{-1}·K and Θ ≈ -1.9 K. χ_o =- 0.418×10^{-6} emu/(Oe·g) was found as a variable fitting parameter.

Spin concentration. According to relatively old literature data, the value of Ns varied in the wide range of 0.5-20×10^{19} spin · g^{-1} [S8], and according to updated data of the last ten years, taken from reliable sources, including ours, it is 5.7-7.3×10^{19} spin · g^{-1} [S1, S9-S11]. Our previous studies started more than 10 years ago showed that the concentration of internal paramagnetic defects (N_s) in DND is practically independent of the types of chemical surface treatment and external doping agents, with the exception of fluorine treatment and etching in aqua regia, and is approximately constant with an accuracy of +-15% for all "standard" DNDs from different manufacturers. This indicates that the majority (~70%) of these defects are buried and located at a distance of more than half a lattice constant from the particle surface. The N_{s_1} value obtained here falls within the range noted above.

S3. Sample irradiation and ESR measurements

The commercial γ-radiation source was purchased from Joint Stock Company 'Svetlana-Semiconductors Devices' (Russia) and consisted of 84 elementary radionuclide ^{137}Cs units of the Gamma Source Cesium 12-1 type installed in a circle, each with an activity of ~2×10^{13} Bq. *Ca.* 85.1% of the ^{137}Cs decays led to γ-ray emission with quanta energy of 0.6617 MeV. The absorption cross section of such a radiation was not enough for the creation of vacancies in diamond. The

doses employed were up to ~13 MGy for ~250 mg sample of the DND-ini powder located on the bottom of a 10 ml glass bottle. The top of the bottle was covered not hermetically with aluminum foil to prevent the dust. No efforts were made to remove air from the radiation chamber. After irradiation the bottle glass became dark.

The ESR spectra were recorded at room temperature at a microwave frequency of ~ 9.5 GHz using an X-band ESR spectrometer JEOL JES-FA 300 (Japan). Powder sample (27.6 mg) was introduced into a quartz tube of 4 mm diameter. Microwave frequency v was 9.4023 GHz, power P_{MW} = 0.03 mW, magnetic field modulation ΔH_m = 0.5 G, modulation frequency 100 kHz, scan time 100 s, temperature 293 K.

S4. Known data on γ-irradiation effect on various carbon materials

Table S1 Various nanocarbons demonstrated the radiation damages, surface functionalization, better mechanical performance or the excellent bioprotection properties under γ-rays exposing.

No.	Material/Refs	Source, dose	Main process	Comment
1	Diamond[S12,13]	γ-rays (1 to 15 MeV)	radiation damage through appearance of vacancies	γ-rays cause damage by generating electrons only for photons with energies above 1-2 MeV
2	Activated carbon[S14]	^{137}Cs, 25 kGy	surface modification	change in surface chemistry by γ-rays and irradiation conditions; irradiation in the air leads to an increase in the percentage of surface oxygen
3	Graphene/carbon nanotube hybrid fillers[S15]	^{60}Co, 300 kGy	polymer chain crosslinking	improvement of mechanical properties and thermal stability of poly (vinyl alcohol) composite films
4	Graphene oxide[S16]	^{60}Co, 50–150 Gy	surface modification	method for turning the physico-chemical properties; radiation-induced functionalization with organosilanes via recombination of radicals
5	Graphene oxide and graphene nanoribbons[S17]	^{60}Co, 60–150 kGy	graphene lattice modification	changes in oxygen content and graphene carbon lattice; restoration of sp^2-hybridized carbon bonds in graphitic structures
6	MEH-PPV/DND nanocomposite[S18]	^{137}Cs, 0.5–12.2 kGy	crosslinking between neighboring groups	crosslinking between DND surface functional groups and polymer chains; polymer stabilization under γ-rays

7	Carboxylated NDs (cNDs)[S19,20]	^{60}Co, 25–60 Gy	cNDs as radical scavengers; the protective effect by neutralizing the free radicals generated during γ- irradiation	indirect protector shield effect and preservation the quality of stored blood following γ-irradiation: better re-oxygenation capability and morphological recovery of irradiated red blood cells (RBC).
8	Hydrogenated NDs[S21]	^{137}Cs, 4 Gy	diosensitizing effect on cancer cells	source of reactive oxygen

References

[S1] V.Yu. Osipov, A.I. Shames, T. Enoki, K. Takai, M.V. Baidakova and A.Ya. Vul', *Diam. Relat. Mater*. 2007, **16**, 2035.

[S2] V.Yu. Osipov, A.E. Aleksenskiy, A.I. Shames, A.M. Panich, M.S. Shestakov and A.Ya. Vul', *Diam. Relat. Mater.*, 2011, **20**, 1234.

[S3] E.-Z. Piña-Salazar, R. Kukobat, R. Futamura, T. Hayashi, S. Toshio, E. Ōsawa and K. Kaneko, *Carbon,* 2018, **139,** 853.

[S4] E.-Z. Pina-Salazar, K. Urita, T. Hayashi, R. Futamura, F. Vallejos-Burgos, J. Włoch, P. Kowalczyk, M. Wiśniewski, T. Sakai, I. Moriguchi, A. P. Terzyk, E. Osawa and K. Kaneko, *Langmuir*, 2017, **33**, 11180.

[S5] E.-Z. Pina-Salazar, K. Sagisaka, Y. Hattori, T. Sakai, R. Futamura, E. Osawa and K. Kaneko, *Chem. Phys. Lett.: X*, 2019, **2**, 100018.

[S6] S. Stehlik, T. Glatzel, V. Pichot, R. Pawlak, E. Meyer, D. Spitzer and B. Rezek, *Diam. Relat. Mater.*, 2016, **63**, 97.

[S7] R.L. Carlin. *Magnetochemistry.* Springer-Verlag, Berlin−Heidelberg−N.Y.−Tokyo, 1986. 328 p.

[S8] A.M. Panich, *Critical Reviews in Solid State and Material Sciences*., 2012, **37**(4), 276.

[S9] *Nanodiamonds: Applications in Biology and Nanoscale Medicine*, Chapter 3. ed. D.Ho, Springer, New York-Dordrecht-Heidelberg-London, 2009. 286 p.

[S10] A.I. Shames, A.M. Panich, V.Yu. Osipov, A.E. Aleksenskiy, A.Ya. Vul`, T. Enoki and K. Takai, *J. Appl. Phys.*, 2010, **107**, 014318.

[S11] *Detonation nanodiamonds: Science and applications*, Chapters 2, 6. eds. A. Vul' and O. Shenderova, Pan Stanford, Singapore, 2014. 346 p.

[S12] B. Campbell, W. Choudhury, A. Mainwood, M. Newton and G. Davies, *Nucl. Instrum. Methods Phys. Res., Sect. A*, 2002, **476**, 680.

[S13] B. Campbell and A. Mainwood, *Phys. Status Solidi A*, 2000, **181**, 99.

[S14] I. Velo-Gala, J. J. López-Peñalver, M. Sánchez-Polo and J. Rivera-Utrilla, *Carbon*, 2014, **67**, 236.

[S15] H.-L. Ma, L. Zhang, Y. Zhang, S. Wang, C. Sun, H. Yu, X. Zeng and M. Zhai, *Radiat. Phys. Chem.*, 2016, **118**, 21.

[S16] K. M. Aujara, B. W. Chieng, N. A. Ibrahim, N. Zainuddin and C. T. Ratnam, *Int. J. Mol. Sci.*, 2019, **20**, 1910.

[S17] A. Ansón-Casaos, J. A. Puértolas, F. J. Pascual, J. Hernández-Ferrer, P. Castell, A. M. Benito, W. K. Maser and M. T. Martínez, *Appl. Surf. Sci.*, 2014, **301**, 264.

[S18] N. M. Romanov, F. M. Shakhov, V. Yu. Osipov and C. F. Musikhin, *J. Opt. Technol.*, 2019, **86**, 608.

[S19] M. Acosta-Elías, A. Sarabia-Sainz, S. Pedroso-Santana, E. Silva-Campa, K. Santacruz-Gomez, A. Angulo-Molina, B. Castaneda, D. Soto-Puebla, M. Barboza-Flores, R. Melendrez, S. Álvarez-García and M. Pedroza-Montero, *Phys. Status Solidi A*, 2015, **212**, 2437.

[S20] K. Santacruz-Gomez, E. Silva-Campa, R. Melendrez-Amavizca, F. T. Arce, V. Mata-Haro, P. B. Landon, C. Zhang, M. Pedroza-Montero and R. Lal, *Nanoscale*, 2016, **8**, 7189.

[S21] R. Grall, H. Girard, L. Saad, T. Petit, C. Gesset, M. Combis-Schlumberger, V. Paget, J. Delic, J.-C. Arnault and S. Chevillard, *Biomaterials*, 2015, **61**, 290.